

# End Space Heat Transfer Coefficient Determination for Different Induction Motor Enclosure Types

A. Boglietti<sup>(1)</sup>, *Senior Member, IEEE*, A. Cavagnino<sup>(1)</sup>, *Member, IEEE*, D.A. Staton<sup>(2)</sup>,

M. Popescu<sup>(3)</sup>, *Senior Member, IEEE*, C. Cossar<sup>(3)</sup>, and M.I. McGilp<sup>(3)</sup>

<sup>(1)</sup> Politecnico di Torino, Dipartimento di Ingegneria Elettrica, 10129 Torino, ITALY

<sup>(2)</sup> Motor Design Ltd, Ellesmere, Shropshire, SY12 OEG, UK

<sup>(3)</sup> SPEED Laboratory, University of Glasgow, Glasgow, G12 8LT, Scotland. UK

**Abstract** – In this paper the determination of the end space induction motor heat transfer coefficients is presented and the methodologies used are examined closely. Two “ad hoc” prototypes have been built and a test bench completed. This paper reports the set up of the test procedures and results obtained in detail.

As the end-windings are the hottest points of the motor particular care has been devoted to the determination of the heat transfer coefficient concerning the end-winding structure. The results obtained are of fundamental importance for the determination of the thermal resistances between end-windings and end caps. These can then be used in thermal networks usually adopted in thermal model analysis.

*Keywords:* induction motors, thermal model, parameter identification, and heat transfer coefficients.

## I. INTRODUCTION

Software for the thermal analysis of induction motors has become popular. When used in conjunction with electromagnetic design provides verification prior to prototype realization. This approach allows a cost saving in progression from the initial design to device production. Additionally, the role of the thermal analysis becomes important in reducing the laboratory time consumed in thermal verification tests.

The accuracy of a thermal analysis is dependant on the accuracy of the thermal resistance computation and, as a consequence, on the accuracy of the available heat transfer coefficients linked to the natural and the forced convection heat exchange inside and outside the motor [1]-[5].

In this paper the end-winding heat transfer coefficient in induction motors have been obtained by means of a full experimental approach supported by thermal analysis with specific thermal models devoted to the electrical machines.

This work is the continuation of the research activity presented in [6] taking into account different motor frames and enclosures and proposing a new thermal model.

After the experimentation and analysis the machine was also modeled in a commercial lumped circuit analysis package for thermal analysis of electric machines [7] and its results compared with the models developed earlier. It gave a good match with the models developed.

## II. THERMAL PHENOMENA AND RELATED PROBLEMS

The thermal phenomena inside an electrical motor are very complex as a great number of thermal exchange phenomena are involved simultaneously. Conduction, natural convection, forced convection and radiation are all present to an extent that depends on the motor cooling system (natural convection, fan cooling, water cooling, and so on). In addition, many heat sources are active at the same time. As a consequence, it is not easy to split the causes and effects in thermal exchange phenomena.

The most widely used procedure to analyze these heat transfer exchange is the definition of thermal networks based on lumped parameters, as shown in the technical literature on this subject [8]-[13]. The difficulty of this approach is the correct computation of heat transfer coefficients and the resulting thermal resistances for convection and radiation heat transfer. When using an experimental approach to help quantify heat transfer coefficients, the use of a standard motor is often not the best choice, in particular when a single thermal effect has to be analyzed [11], [14], [15]. As a consequence, in the proposed approach, suitable induction motor prototypes have been designed and built [16], [17].

## III. TEST BENCH AND MOTOR PROTOTYPES

On the basis of the authors’ experiences, the thermal phenomena analysis can be improved in a system where, as far as possible, the heat sources can be separately activated. In particular, when the stator winding cooling effects are under analysis as a function of the rotor speed, it is convenient that only the stator joule losses should be present and the other thermal sources should not be active. This condition is particularly true when the phenomena involved in the end-winding cooling have to be studied [6].

For this reason, two “ad hoc” prototypes have been built. The first prototype is a standard 2 poles Total Enclosed Fan Cooled “TEFC” motor (in the following labeled as Motor A), while the second one is a 4 poles Open Drip Proof “DP” (in the following identified as Motor B). In this motor some openings are present in the main frame and in the two end-caps for increasing the cooling effects of the end-windings.

TABLE I  
PROTOTYPES NAME PLATE DATA

Motor prototype	Motor A	Motor B
Original motor rated power [HP]	3	5
Enclosure type	TEFC	DP
Frequency [Hz]	60	60
Rated Voltage [V]	230/460	230/460
Rated current [A]	8.0/4.0	13.4/6.7
Pole number	2	4
Rated speed [rpm]	3530	1760
Rated efficiency [%]	88.5	87.5

In both the motors, the rotor laminations and the rotor squirrel cages have been totally replaced by a plastic cylinder. The two cylinders replacing the original rotors are made of Nylon. In order to maintain the internal ventilation effect, the two end-rings of the original rotors have been fixed on the two sides of the plastic cylinder. The plastic rotor diameter has been turned to maintain the same value of the original one. The adopted motor code together with the name plate data of the two prototypes are reported in Table I. Fig.1 shows the TEFC Motor A, Fig.2 show the DP Motor B, while Fig.3 shows the two prototypes “plastic” rotors. In the bigger rotor (Motor B), very long end-ring fins are adopted (as evident in Fig.3) to improve the end-windings ventilation. Conversely, the small rotor (Motor A) has regular end-ring fins, as usual in this machine type. As a consequence, it could be expected that the two machines would have different behavior concerning the end windings cooling effects.

The two motors are not thermally monitored by thermal sensors, but the winding temperatures can be self monitored during the tests as described in section IV, while the stator lamination temperature can be measured by a digital thermometer through the openings available in the frame for Motor B and a hole available inside the terminal box for Motor A. The test bench used is shown in Fig.4. Obviously, due to the plastic rotors, the two motors cannot rotate by themselves, so the two rotors are mechanically connected to an industrial TEFC induction motor (in the following the Drive Motor) using the mechanical output shafts of this machine. In particular, the regular output shaft is connected to one motor under test while the shaft on the other side is connected to the second prototype removing the external fan and cowling of the Drive Motor. The two motors under test have both been connected to the Drive Motor because this configuration allows performing the thermal tests on the two machines at the same time, halving the number of tests.

The two mechanical joints between the three motors have been realized using a simple rubber water-pipe. This choice is possible because only the very small torque due to the mechanical losses is involved. In addition, the rubber water-pipe introduces a high thermal resistance between the three shafts forming a thermal disconnection which thereby reduces the thermal flux from one motor to the other one. In this way, the three motors can be considered thermally decoupled. This configuration minimizes the ventilation effects on the prototype endcaps that could be introduced by traditional mechanical joints.



Fig. 1: Motor A (2 poles TEFC machine).



Fig. 2: Motor B (4 poles DP machine).

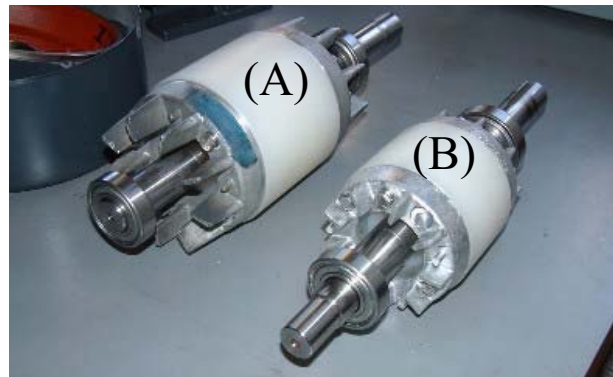


Fig. 3: Plastic rotors used for the tests.



Fig. 4: Test bench with the two motors under test.

In order to increase the thermal decoupling, a plastic barrier is introduced between the Drive Motor and Motor A, as shown in Fig.4. The aim of the plastic barrier is to stop the air flow produced by Motor B versus Motor A. An inverter is used to supply the Drive Motor, in order to impose the requested speed to the two plastic rotors. The test bench has been positioned in a room with ambient temperature variation lower than 2 °C throughout the day. The test rig has been position on a wood support to reduce the thermal exchange through the motor feet.

#### IV. EXPERIMENTAL TESTS AND RELATED RESULTS

Using the previously described test bench the following tests have been performed on each prototype:

- Thermal test with a DC supply connecting the three windings in series and with the rotor still. This test is the reference condition for the thermal models set up.
- Thermal test with a DC supply connecting the three windings in series and with the rotor running at constant speed imposed by the driven motor. In particular the following mechanical speeds have been considered: 250, 500, 750, 1000, 1500, 2000, 2500 rpm.

Motor B has been included in the tests at speeds greater than which it is rated for in order to have experimental data in as large as possible a speed range.

The use of a DC supply involves the stator joule losses only, simplifying the thermal analysis. In fact, with a sinusoidal supply, the loss contribution values are not known accurately (the loss separation is made following international standards, i.e. [18], [19]). In DC supply conditions the thermal system is more obvious and an easier thermal analysis can be adopted. In addition, knowing the winding resistance at a reference temperature with a DC supply, the ratio between the voltage and current allows continuous monitoring of the winding temperature during the test up to the thermal steady state condition.

In order to avoid motor damage, the supply voltage for the two motors has been chosen to supply a constant DC injected power (100 W for Motor A and 150 W for Motor B) suitable for a temperature rise of about 70 °C for both the prototypes taking into account the motor insulation class. It is important to remember that during the DC test with the rotor still the prototypes are without any type of ventilation.

In the tests, the stator winding, stator lamination and external motor frame temperatures have been measured in thermal steady state condition, together the ambient temperature. The external motor frame temperature is the average values of 25 measured temperatures on the main frame and on the end-caps (see Fig. 5).

Fig. 6 (Motor A) shows that the winding temperature is constantly decreasing, while for rotor speeds higher than 1500 rpm, the stator lamination and the motor frame temperature tend to increase. This trend can be justified by the increase of the bearing mechanical losses with the increase in speed and the increase of the ventilation losses inside the closed end-caps.

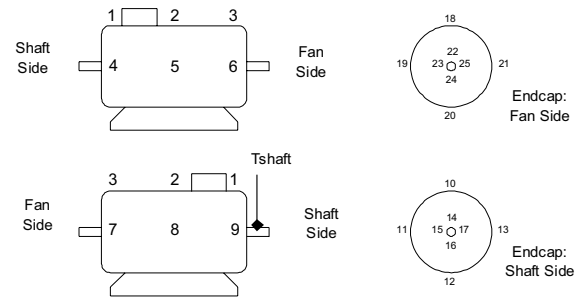


Fig. 5: Temperature measurement points on the external frame.

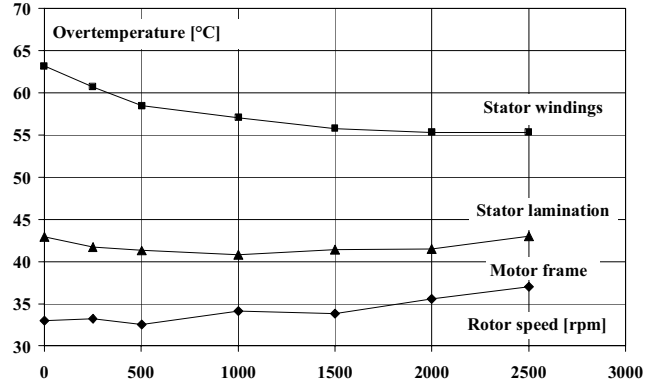


Fig. 6: Stator winding, stator lamination and external motor frame over temperature versus the rotor speed for the Motor A.

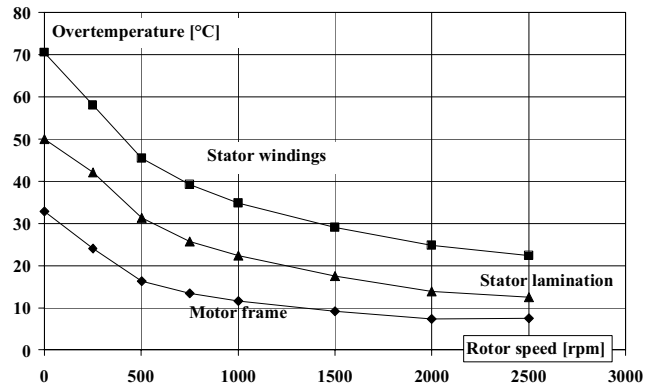


Fig. 7: Stator winding, stator lamination and external motor frame over temperature versus the rotor speed for the Motor B.

It is important to underline that the air inside the end-caps is whirled by the end-ring fins and pins.

For Motor B (Fig. 7) it is evident that there is a reduction of all the temperatures with the speed increase. In this case it is important to remember that the motor frame is open with effective cooling and air exchange due to the fan effects of the endring fins. As discussed in section VI, for Motor B the heat removal through the frame opening is considerable.

#### V. MOTOR A THERMAL ANALYSIS

As Motor A is a TEFC machine, its thermal behavior can be analyzed by means of a very simplified thermal network proposed and discussed in [6].

TABLE II  
MEANING OF THE THERMAL COMPONENTS IN FIG.8

Symbol	Meaning
$P_S$	Stator winding joule losses (active conductors in the slots)
$P_{EW}$	Stator winding losses (end windings)
$R_0$	Thermal resistance between motor frame and ambient
$R_{S-MF}$	Thermal resistance between copper in the slot and rotor frame
$R_{NC}$	Thermal resistance between endwindings and motor frame due to natural convection
$R_{RAD}$	Thermal resistance between endwindings and motor frame due to radiation
$R_{EW-IA}$	Thermal resistance between endwindings and the inner air
$R_{IA-MF}$	Thermal resistance between inner air and the motor frame

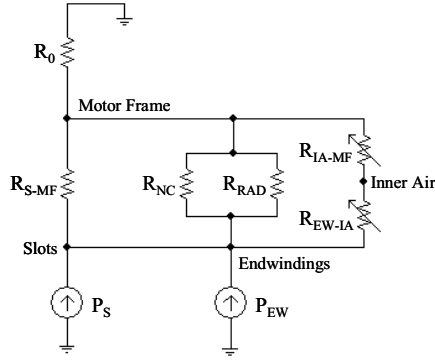


Fig. 8: Equivalent thermal network (Model 1).

For convenience aims, the equivalent thermal circuit proposed in [6] (in the following Model 1) is reported in Fig. 8 and the meaning of the used symbols is listed in Table II. This thermal network can be used to determine the thermal resistances starting from the measured temperature rises in the different machine parts.

#### A. Thermal Resistance Estimation

In the following the step-by-step procedure for the thermal resistance computation is reported.

First of all, it is important to underline that from the measured results the thermal resistance  $R_0$  is practically constant at the different speeds (see Fig. 6). In fact, with a constant injected DC power in the winding, the measured motor frame temperature rise was practically constant at all the rotor speeds. As a consequence, the value of this thermal resistance has been considered constant for the computation of the other thermal resistances used in Model 1.

1. As previously reported the thermal resistance  $R_0$  is independent of the rotor speed and can be computed by (1).

$$R_0 = \frac{\Delta T_{MF}}{P_S + P_{EW}} = 0.3341 \text{ } ^\circ\text{C/W} \approx \text{constant} \quad (1)$$

2. The thermal resistance  $R_{S-MF}$  has been computed using two different thermal models [9], [12]. As discussed in these references, both the models provided the same

results with a good accuracy. For the motor A the obtained value is  $R_{S-MF} = 0.4728 \text{ } ^\circ\text{C/W}$ .

3. The equivalent thermal resistance between the stator winding and the motor frame ( $R_{S-MF}$ ), is dependant on the rotor speed and can be computed by (2).

$$R_{S-MF} = \frac{\Delta T_{SW} - \Delta T_{MF}}{P_S + P_{EW}} \quad (2)$$

4. The equivalent thermal resistance between end winding and motor frame (due to natural convection, radiation and forced convection) can be determined by (3).

$$R_{EW-MF} = \frac{1}{\frac{1}{R_{NC}} + \frac{1}{R_{RAD}} + \frac{1}{(R_{EW-IA} + R_{IA-MF})}} = \frac{1}{\frac{1}{R_{S-MF}} - \frac{1}{R_{S-MF}}} \quad (3)$$

5. The addition of the thermal resistance between end winding and inner air plus the thermal resistance between inner air and motor frame ( $R_{EW-IA} + R_{IA-MF}$ ) is defined as

$$R_{EW-IA} + R_{IA-MF} \Big|_{n>0} = \frac{1}{\frac{1}{R_{S-MF} \Big|_{n>0}} - \frac{1}{R_{S-MF} \Big|_{n=0}}} \quad (4)$$

where  $n$  is the rotor speed in rpm.

The computed values of the thermal resistance between stator winding and motor frame and of the thermal resistance between end winding and motor frame as a function of the rotor speed are reported in Fig. 9 and Fig. 10 respectively.

#### B. Heat transfer coefficients

Hereafter the procedure for the computation of the heat transfer coefficient for the end-windings is reported.

1. The involved areas have to be computed for example following the procedure reported in [6]. For Motor A the value of the end-winding area  $S_{EW}$  is  $0.1546 \text{ m}^2$  and the value of the end-caps area  $S_{EC}$  is  $0.1039 \text{ m}^2$ .
2. After the area computations it is possible to determine the heat transfer coefficient between the endwindings and the inner air “ $h_{EW-IA}$ ” and between the inner air and the frame “ $h_{IA-MF}$ ”. Since the temperature of the inner air was not measurable, the computation of separate values for “ $h_{EW-IA}$ ” and “ $h_{IA-MF}$ ” was not possible. As a consequence, the two heat transfer coefficients are considered equal  $h_{EW-IA} = h_{IA-MF} = h$ . The use of different values for these two coefficients can be found in [20].
3. The equivalent heat transfer coefficient (taking into account natural convection, radiation and forced convection) is computed by the thermal resistance  $R_{EW-MF}$  using (5). This means that the resulting straight line by the linear fitting must not cross the axis origin. In fact the intercept with the vertical axis is related to the natural convection and radiation.

$$h_{\text{Equivalent}} = \frac{1}{R_{EW-MF}} \left( \frac{1}{S_{EW}} + \frac{1}{S_{EC}} \right) \quad (5)$$

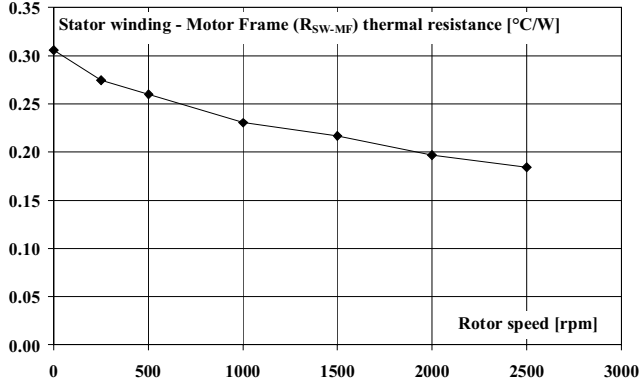


Fig. 9: Thermal resistance between stator winding and motor frame vs. rotor speed (Motor A).

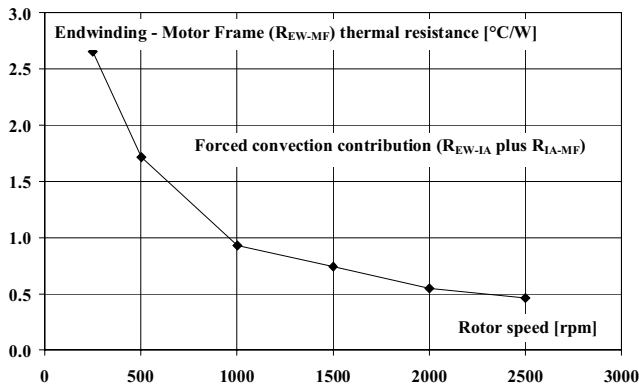


Fig. 10: Thermal resistance between end-winding and motor frame vs. rotor speed (Motor A).

4. The heat transfer due to the forced convection is determined from the series of the thermal resistances  $R_{EW-IA}$  and  $R_{IA-MF}$  by (6). In this case the straight line produced by a linear regression should cross the axis origin. The obtained results are reported in Fig.11, where the heat transfer straight line intercept with the vertical axis is very small highlighting the good accuracy of the computed results.

$$h_{\text{Forced Convection}} = \frac{1}{R_{EW-IA} + R_{IA-MF}} \left( \frac{1}{S_{EW}} + \frac{1}{S_{EC}} \right) \quad (6)$$

## VI. MOTOR B THERMAL ANALYSIS

### A. Thermal Resistance Estimation by Model 1

As for Motor A, the value of the thermal resistance  $R_0$  has been computed using (1) and the obtained values are reported in Fig.12. The trend reported in Fig.12 could lead to considering a reduction of the thermal resistance  $R_0$  with the rotor speed, but this does not seem correct from the physic point of view. In fact, using the thermal Model 1 the heat removal by the air flux due to the end ring fin rotation is associated to the thermal resistance  $R_0$ .

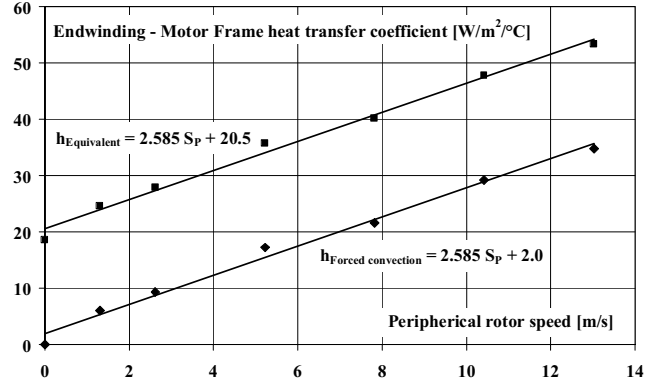


Fig. 11: Endwinding – Motor frame heat transfer coefficient (Motor A).

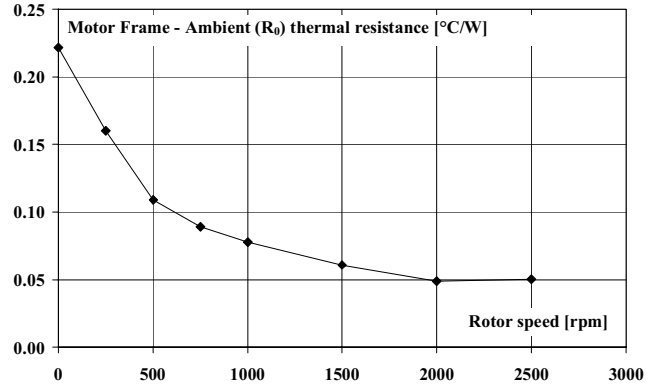


Fig. 12: Thermal resistance between motor frame and ambient  $R_0$  (Motor B).

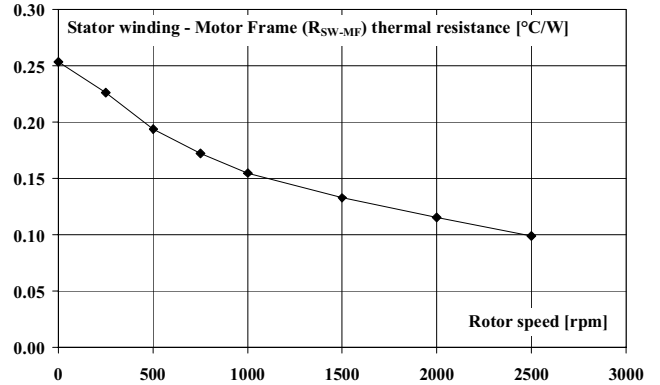


Fig. 13: Stator winding-motor frame thermal resistance (Motor B).

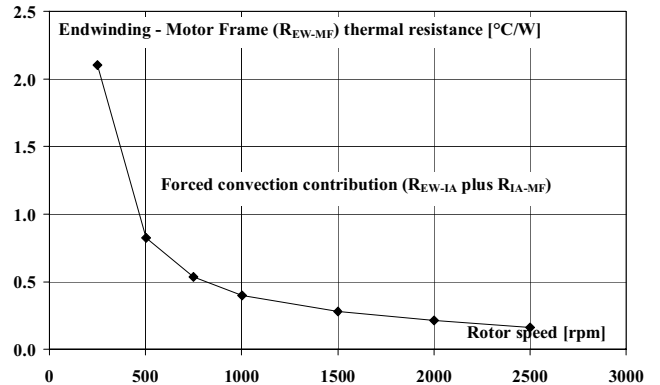


Fig. 14: Endwinding - motor frame thermal resistance (Motor B).

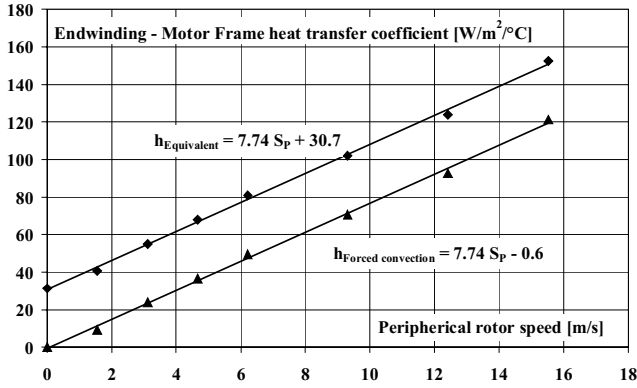


Fig.15: End-winding – Motor frame heat transfer coefficient for the Motor B.

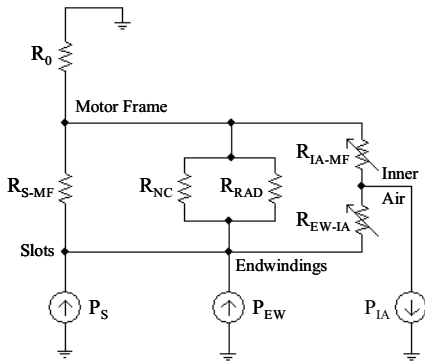


Fig.16: Equivalent thermal network (Model 2)

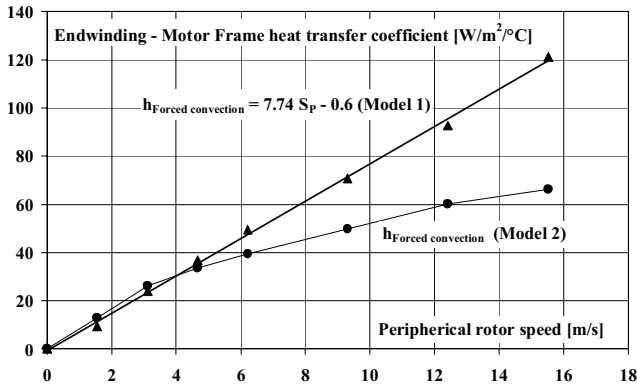


Fig. 17: End-winding – Motor frame heat transfer coefficient comparison using Model 1 and Model 2 for the Motor B.

Nevertheless, using the thermal Model 1 and the same step-by-step approach described for the Motor A, it is possible to compute the thermal resistances for the Motor B too. The following data have been considered in the calculations:  $R_{S-MF} = 0.4253 \text{ } ^\circ\text{C/W}$ ,  $S_{EW} = 0.1332 \text{ m}^2$  and  $S_{EC} = 0.0820 \text{ m}^2$ . The obtained results are reported in Fig.13 and Fig.14. In Fig.15 the heat transfer coefficient for Motor B, computed following the same approach used for Motor A, is reported. Even if the values and the trends reported in Fig.15 can be reasonable, the heat removal through the frame opening is not modeled in the correct way with the reduction of the thermal resistance  $R_0$ .

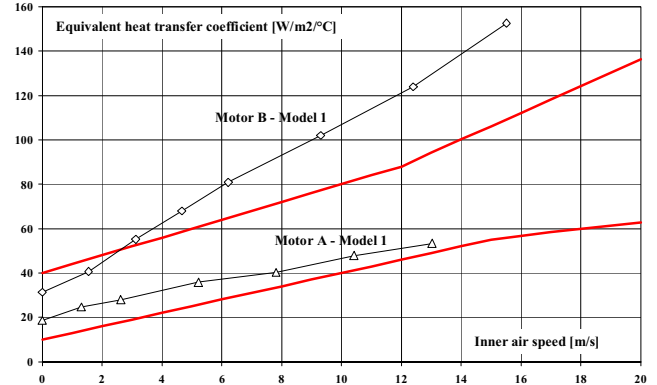


Fig. 18: Comparison between the obtained equivalent heat transfer coefficients for the two prototypes and the values reported in literature.

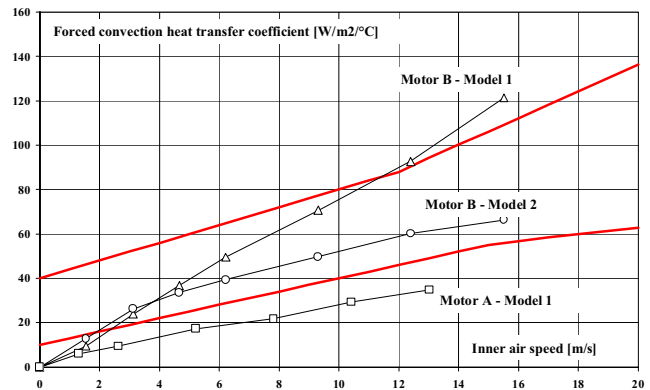


Fig. 19: Comparison between the obtained forced convection heat transfer coefficients for the two prototypes and the values reported in literature.

### B. Thermal Resistance Estimation by Model 2

A modification of the thermal network has been adopted in order to better match the model with the involved physic phenomena. In the following the new proposed thermal model, reported in Fig.16, will be identified as Model 2. In the new thermal model an additional power generator “ $P_{IA}$ ” is connected in the “inner air node”. This power generator has to take into account the heat removed through the frame opening by air flux produced by the rotating end-ring fins. As supposed for Model 1 similarly for Model 2 the thermal resistance  $R_0$  has been considered constant (equal to the measured one with the rotor still,  $R_0 = 0.2216 \text{ } ^\circ\text{C/W}$ ) with respect to the rotor speed. As a consequence, the value of  $P_{IA}$  can be evaluated by the power balance and the heat flux in  $R_{EW-IA}$  and  $R_{IA-MF}$  can be consequently obtained. Assuming again  $h_{EW-IA} = h_{IA-MF}$  it is possible to identify the heat transfer coefficient values reported in Fig. 17. As shown in Fig.17, it is evident that Model 2 produces a non linear variation of the heat transfer coefficient with respect to the rotor speed. This trend can be justified, considering that an increase of the rotor speed and consequently of the inner air flow through the frame openings, does not correspond to a proportional increase of the heat removal by the forced convection in the end space.

In Fig.18 and Fig.19 the comparison between the obtained heat transfer coefficients for Motor A and Motor B

respectively, to values reported in literature is shown. In these figures, the previously published heat transfer coefficient correlations are inside the region between the two continuous red lines [6].

It is important to take into account that Motor B is not a TEFC machine so the comparison has to be considered in a qualitative way.

### VII. COMMERCIAL THERMAL ANALYSIS SOFTWARE MODEL

The two prototype motor geometries were input into the commercial thermal analysis software [7]. This included the nylon rotor and fixed values of copper losses for the two motors. Simulations were made at the different shaft speeds that measurements were made.

Default values maintained in the software for all parameters such as interface gaps between components, convection heat transfer coefficients for the housing (calculated from convection corrections for the particular frame geometry), etc. Such data is set up in the software to represent typical values found in electric motors so that the user need not be a thermal expert to obtain reliable results (i.e. the interface gap between the stator lamination to housing is usually larger than that found between non laminated surfaces [4]).

A comparison between the predicted and measured winding, stator lamination and housing (node 2 in Fig 5) temperatures are shown in Fig. 20 and Fig. 21 for motors A and B respectively. It is seen that there is a high level of agreement for both motors. The heat transfer coefficient for all surfaces within the endcaps is calculated using the default method implemented in the software. This is the relationship of Schubert, which is detailed in [4]:

$$h = 15 \cdot \left[ 1 + (0.4 \cdot vel)^{0.9} \right] \quad (7)$$

It has a natural convection term and a forced convection component that is a function of the local air velocity (*vel* in m/s). In a total enclosed machine as in motor A the local air velocity over the end-winding surfaces is related to the rotor peripheral velocity, which is a function of the rotational speed. A scaling factor (endwinding fanning factor in Fig. 22) is used in the software to directly relate the magnitude of rotational air velocity in the endcaps to the rotor peripheral velocity.

If the internal fan is large the internal air velocity will be close to the rotor peripheral velocity and the end-winding fanning factor should be made equal to 1. If there is no internal fan and the ends of the rotor are smooth the internal air velocity will be much less and the end-winding fanning factor will be closer to 0. Values of end-winding fanning factor equal to 0.8 and 1.0 were used for motors A and B respectively.

A larger value was used for motor B as it has larger wafters incorporated into the rotor end rings. It is seen that for motor A the results are not too sensitive to the correct selection of the end winding fanning factor so only a rough estimate is required.

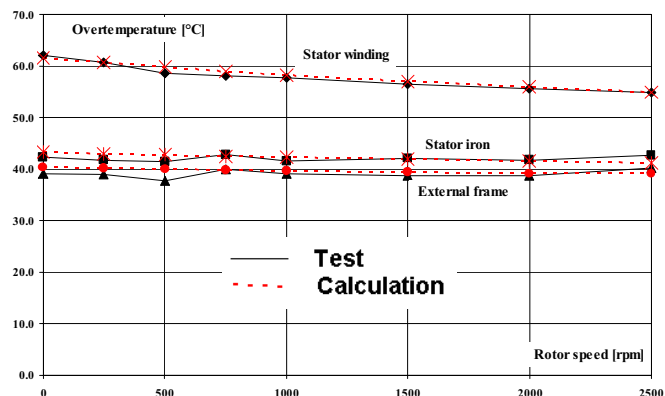


Fig. 20: Commercial software prediction and measured winding, stator lamination and frame temperature rise versus the rotor speed (Motor A).

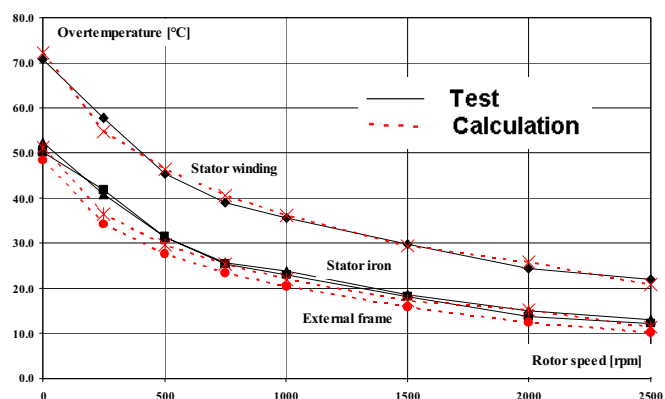


Fig. 21: Commercial software prediction and measured winding, stator lamination and frame temperature rise versus the rotor speed (Motor B).

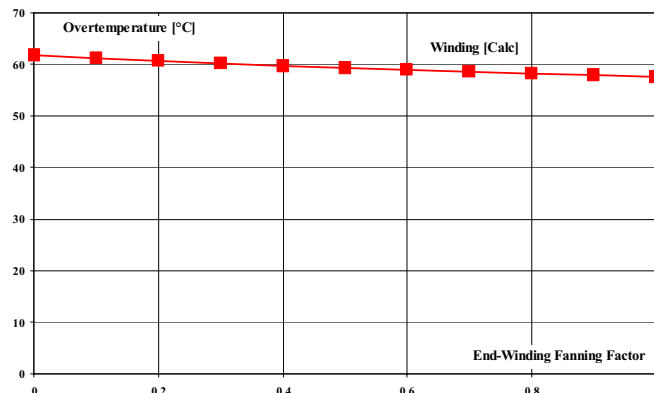


Fig. 22: Motor A winding temperature rise versus the selection of the end winding fanning factor.

Motor B has opening in the endcaps which are modeled in the software. They have two major cooling effects which are taken account of in the simulation:

- The effect of the external air entering the machine reducing the internal ambient. The amount of air entering the machine is proportional to the rotational speed according to fan scaling laws. In this case the fan forcing air into the machine is attached to the rotor (wafters on the end rings). The predicted internal air

temperature in the machine as a function of rotational speed is shown in Fig 23.

- The increase in air velocity over end winding and internal surfaces of the endcaps and housing due to air entering the machine. The local velocity over a surface is a function of the air entering the machine and the rotational velocity.

The drip proof motor is slightly more complex to model accurately than the totally enclosed machine as the user must provide an estimate of the volume flow rate entering the machine at one rotor speed. The volume flow rate at other speed is calculated assuming flow is proportional to speed as indicated by fan scaling laws.

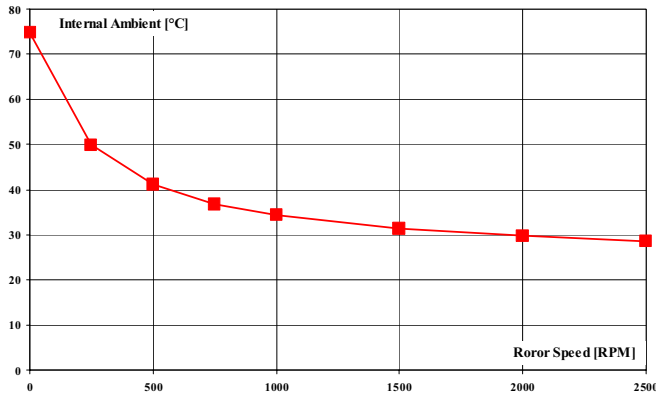


Fig. 23: Predicted internal ambient as a function of rotor speed for Motor B.

### VIII. CONCLUSIONS

The method of testing induction machines with nylon rotors with the end-ring and wafers still in place and a dc current in the stator winding has proved useful for identifying heat transfer coefficients and thermal resistances associated with the end windings. In particular, the proposed method has been successful applied to two induction motor prototypes with different enclosures. For each considered machine, a simplified thermal model suitable to describe its thermal behavior have been proposed and deeply discussed. Finally, the endwinding-motor frame thermal resistances and the related heat transfer coefficients have been identified on the bases of experimental tests.

The commercial thermal analysis software gave a good prediction of the winding, stator lamination and housing temperatures for both the totally enclosed and drip proof machines. This was with default settings for most parameters in the software. For the totally enclosed machine a setting of 0.8 was used for the end winding fanning factor to account for the fact that a medium size end ring wafting fan is used. The drip proof motor has a larger wafter fan so a value of 1 was used. It was shown that the resulting temperature prediction was not too sensitive to the selection of the end winding fanning factor so a very rough estimate can be made by the user and accurate result still obtained. The drip proof motor is slightly more complex to model accurately as the user must provide an estimate of the volume flow rate entering the machine.

### ACKNOWLEDGMENTS

The authors would like to thank Alan Barker, Steve Ruffing and Alan Crapo of Emerson Motors, St. Louis, USA, for the support of this project. We would also like to acknowledge the assistance of Peter Miller of the *SPEED* Laboratory.

### REFERENCES

- [1] D. Staton, S.J. Pickering, D. Lampard, "Recent Advancement in the Thermal Design of Electric Motors", SMMA 2001 Fall Technical Con., Durham, North Carolina, 3-5 Oct. 2001
- [2] D. Staton, "Thermal analysis of electric motors and generators", Tutorial course IEEE IAS Annual Meeting 2001, Chicago, USA.
- [3] J.R. Simonson, "Engineering Heat Transfer" 2<sup>nd</sup> Edition, McMillan, 1998.
- [4] D. Staton, A. Boglietti, A. Cavagnino, "Solving the More Difficult Aspects of Electric Motor Thermal Analysis, in small and medium size industrial induction motors", *IEEE Transaction on Energy Conversion*, Volume 20, issue 3, September 2005, pp.620-628.
- [5] A. Boglietti, A. Cavagnino, D. Staton, "TEFC Induction Thermal Models: A Parameters Sensitivity Analysis", *IEEE Transactions on Industry Applications*, Volume 41, Issue 3, May-June 2005, pp. 756 – 763.
- [6] A. Boglietti, A. Cavagnino, "Analysis of the Endwinding Cooling Effects in TEFC Induction Motors", *IEEE Transactions on Industry Applications*, Volume 43, Issue 5, Sept.-Oct. 2007, pp.1214 – 1222.
- [7] Motor-CAD, available on [www.motor-design.com](http://www.motor-design.com)
- [8] P. Mellor, D. Roberts, D. Turner, "Lumped parameter thermal model for electrical machines of TEFC design", *IEE Proceedings*, Volume 138, September 1991.
- [9] A. Boglietti, A. Cavagnino, M. Lazzari, M. Pastorelli, "A simplified thermal model for variable speed self cooled industrial induction motor", *IEEE Transactions on Industry Application*, Volume 39, Issue 4, pp.945-952.
- [10] D.A Staton, "Thermal Computer Aided Design" - Advancing the Revolution in Compact Motors, conf. Rec. IEEE-IEMDC 2001, Boston, USA, June 2001.
- [11] A. Boglietti, A. Cavagnino, M. Parvis, A. Vallan, "Evaluation of radiation thermal resistances in industrial motors", *IEEE Transactions on Industry Applications*, Volume 42, Issue 3, May/June 2006, pp. 688-693.
- [12] A. Boglietti, A. Cavagnino, D. Staton, "Thermal Analysis of TEFC Induction Motors", conf. Rec. IEEE-IAS'03, Annual Meeting, 12 – 16 October 2003, Salt Lake City, USA, Volume 2, pp. 849-856.
- [13] A. Cavagnino, D. Staton, "Convection Heat Transfer and Flow Calculations Suitable for Analytical Modelling of Electric Machines", CD Conf. Rec. IECON07, 6-10 November 2006, Paris, France, pp. 4841-4846.
- [14] J. Muggleston, S.J. Pickering, D. Lampard, "Effect of Geometry Changes on the Flow and Heat Transfer in the End Region of a TEFC Induction Motor", 9th IEE Intl. Conf. Electrical Machines & Drives, Canterbury, UK, Sept 99.
- [15] M.A Valenzuela, J.A. Tapia, "Heat Transfer and Thermal Design of Finned Frames for TEFC Variable Speed Motors", CD Conf. Rec. IECON07, 6-10 November 2006, Paris, France.
- [16] T.J.E. Miller, M.I. McGilp, M. Oлару. "PC-FEA 5.5 for Windows – Software", *SPEED Laboratory*, University of Glasgow, Glasgow (UK), 2006
- [17] T.J.E. Miller, and M.I. McGilp "PC-IMD 4.0 for Windows–Software", *SPEED Laboratory*, University of Glasgow, Glasgow (UK), 2007
- [18] IEEE Std 112-2004, "Standard Test Procedure for Polyphase Induction Motors and Generators", New York, Institute of Electrical and Electronics Engineers, 2004.
- [19] IEC 61972 Standard, "Method for Determining Losses and Efficiency of Three-Phase Cage Induction Motors", 2002.
- [20] C. Micallef, S.J. Pickering, K.A. Simmons, K.J. Bradley, K.J., "An Alternative Cooling Arrangement for the End Region of a Totally Enclosed Fan Cooled (TEFC) Induction Motor", *IEE conference on Power Electronics, Machines and Drives PEMD 08*, 3-5 April 2008, York, UK.